SOFT ROBOTICS
Volume 00, Number 00, 2023

DOI: 10.1089/soro.2022.0132

SoRo
Soft Robotics

Strong Reliable Electrostatic Actuation Based on Self-Clearing Using a Thin Conductive Layer

Guoyong Xie,[1,*] Dongliang Fan,[1,2,*] Huacen Wang,[1,2] Renjie Zhu,[1,2] Jianjun Mao,[2] and Hongqiang Wang[1–3]

Abstract

Electrostatic adhesion, as a promising actuation technique for soft robotics, severely suffers from the failure caused by the unpredictable electrical breakdown. This study proposes a novel self-clearing mechanism for electrostatic actuators, particularly for electrostatic adhesion. By simply employing an enough thin conductive layer (e.g., <7 μm for copper), this method can spontaneously clear the conductor around the breakdown sites effectively once breakdowns onset and survive the actuator shortly after the electrical damage. Compared with previous self-clearing methods, which typically rely on new specific materials, this mechanism is easy to operate and compatible with various materials and fabrication processes. In our tests, it can improve the maximum available voltage by 260% and the maximum electrostatic adhesive force by 276%. In addition, the robustness and repeatability of the self-clearing mechanism are validated by surviving consecutive breakdowns and self-clearing of 173 times during 65 min. This method is also demonstrated to be capable of recovering the electrostatic pad from severe physical damages such as punctures, penetrations, and cuttings successfully and enabling stable and reliable operation of the electrostatic clutch, or gripping, for example, even after the short-circuit takes place for hundreds of times. Therefore, the proposed self-clearing method sheds new light on high performance and more extensive practical applications of electrostatic actuators in the future.

Keywords: electrostatic adhesion, self-clearing, electrostatic actuator, fault tolerance

Introduction

As an emerging promising attachment technique, electrostatic adhesion has been extensively applied in soft robots,[1–5] flying vehicles,[6,7] wearable devices,[8–12] grippers,[13–17] and aerospace applications.[18] Usually, it is composed of a conductive pad and an electroadhesive pad (EPad) consisting of a conductive layer covered by insulation, as shown in Figure 1A. Supplied with a high voltage, dislike charges induced in the conductive layer and the conductive pad generate attractive force. Compared with other adhesion methods,[19–21] electrostatic adhesion is lightweight, low cost, energy efficient, deformable, and quickly responsible.[22,23]

Nevertheless, the EPad suffers from unpredictable electrical breakdown, which severely limits its practical applications. Once a short circuit happens accidentally, the whole

[1]Shenzhen Key Laboratory of Biomimetic Robotics and Intelligent Systems, Department of Mechanical and Energy Engineering, Southern University of Science and Technology, Shenzhen, , China.
[2]Guangdong Provincial Key Laboratory of Human-Augmentation and Rehabilitation Robotics in Universities, Southern University of Science and Technology, Shenzhen, China.
[3]Southern Marine Science and Engineering Guangdong Laboratory (Guangzhou), Guangzhou, China.
*These authors contributed equally to this study.

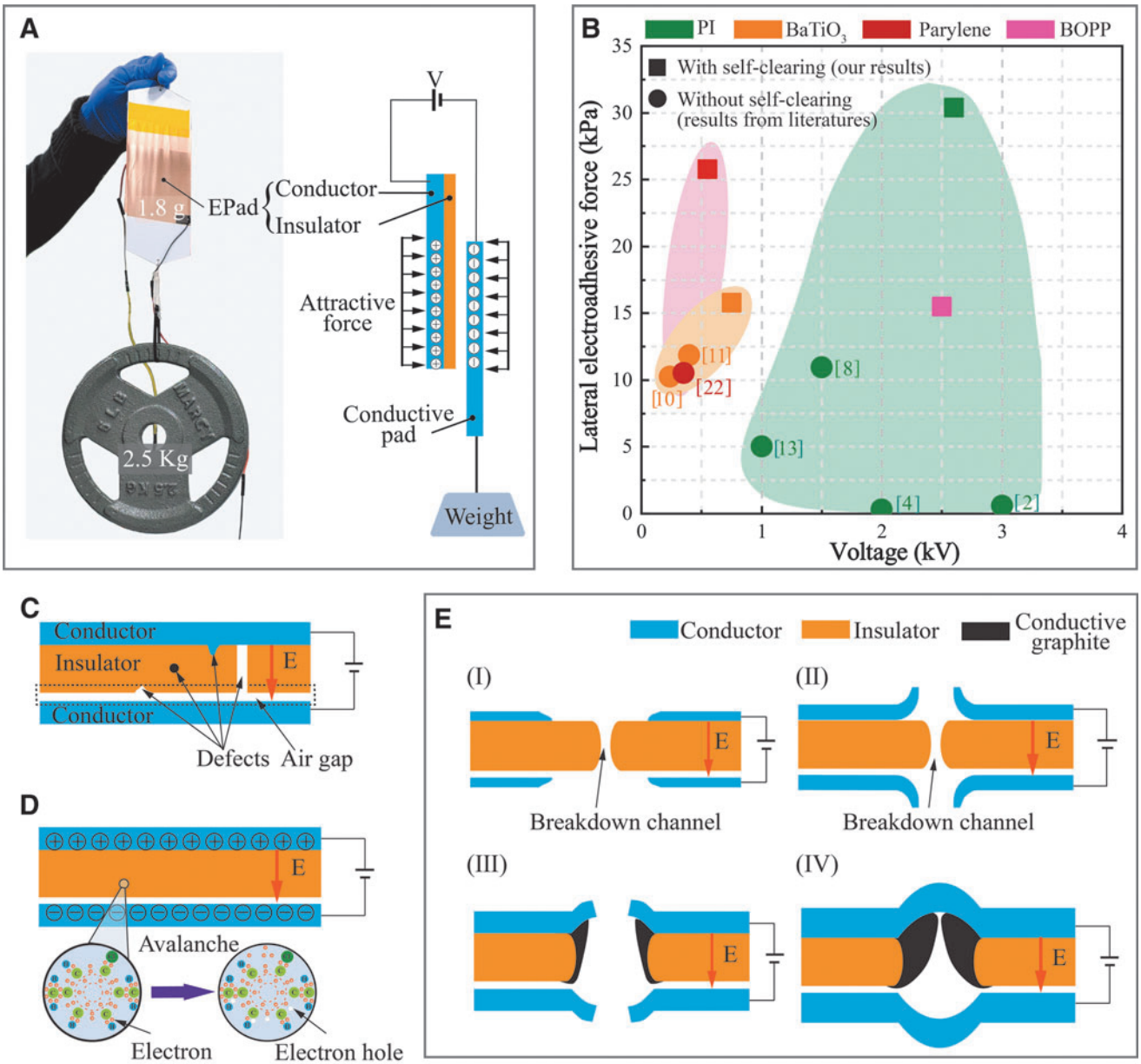

FIG. 1. The mechanism of electrostatic adhesion and its self-clearing based on the thin conductive layer. **(A)** The principle of electrostatic adhesion. The electrostatic adhesion is demonstrated by a 1.8 g electrostatic clutch while holding a 2.5 kg dumbbell. **(B)** The force of electrostatic adhesion using self-clearing (this study, squared markers) and others without self-clearing (previous literature, circle markers). Colors indicate different materials. **(C)** Schematic drawing of defects in the electrode, including foreign particles, heterogeneous crosslinking, uneven thickness, and holes. **(D)** Schematic of the electronic avalanche. **(E)** Four self-clearing hypothesis modes.

device fails suddenly and cannot recover back.[24] The breakdown is hard to predict since most of the discharge is caused by the defects embedded in the dielectric materials, and these defects may be presented during material preparation, including foreign particles, heterogeneous crosslinking, and uneven thickness, or presented in the process of manufacture and operation, such as stress concentration, breakdown puncture, and void formation.[25]

In practice, to avoid electrical breakdown, the voltage is restricted to a magnitude much lower than the threshold acquired from tests and theories, and consequently, the adhesive force that is proportional to the square of the voltage drops drastically.

We found that by simply thinning the conductive layer, the EPad can survive defect-driven premature unrecoverable breakdown damage and prolong the lifetime of EPads. A thinner conductive layer in an EPad allows the arc energy during discharge to be adequate to evaporate and deform the local electrode. This self-clearing phenomenon recovers the circuit shortly after the onset of breakdown, and the EPad becomes available again. Until now, the research on electroadhesion has taken little advantage of fault-tolerant techniques as far as we know.[26,27]

Other studies on electrostatic actuators (e.g., dielectric elastomer actuators) have employed single-walled carbon nanotubes and dielectric liquids as the conductive layer and insulation layer, respectively, for localized clearing, but they

are high cost or complicated in manufacturing.[27,28] By the method proposed in this study, however, we do not need to change the materials and fabrication processes, but just simply keep the thickness of the conductor under a certain value (e.g., approximately <7 μm for copper). Hence it is easy to operate and compatible with existing materials and fabrication processes, as shown in Figure 1B.

Moreover, self-clearing can also be used to remove defects to achieve a higher critical voltage and adhesive force (that is proportional to the square of the voltage). As shown in Figure 1B, based on the self-clearing mechanism, the EPad in this study can sustain a higher electrical field in practice and achieve an output force >270% times higher than previous study using the same materials.

Materials and Methods

To verify the manufacturing compatibility of the self-clearing mechanism proposed here, we demonstrated a series of EPads using different materials and fabrication methods (Fig. 2). We employed LuxPrint, poly-p-dichlorotoluene (Parylene C), polyimide (PI), poly(vinylidene fluoride–trifluoroethylene–chlorotrifluoroethylene) [P(VDF-TrFE-CTFE)] film, and biaxially oriented polypropylene (BOPP), respectively, as the insulator, and copper, aluminum, and carbon nanotubes as the conductor in the EPads. We fabricated the EPads by chemical vapor deposition (CVD), screen printing, electroplating, and heat pressing, respectively, according to the materials. Most of these materials and fabrication methods are extensively applied in the mass production of flexible circuits.

The parylene insulation layer was generated in a coating machine (PTP-3V; Penta). This fabrication method, as shown in Figure 2A, includes the following three steps: Dimer C in the glass tank of the sublimation furnace is first heated to evaporate at 120°C; then, the gas is pyrolyzed into a monomeric form in the pyrolysis furnace at 680°C; finally, the monomer gas runs into the deposition chamber under ambient temperature and deposits as a thin coating layer on the surface of the samples (conductor films). A silane coupling agent (KH-570) was added to the deposition chamber to enhance the bonding strength of the coating layer. This CVD method can generate a uniform thickness pinhole-free coverage on all the surfaces of a conductor, including the edges, and ensure perfect insulation.

The PI insulation layer in this study was bonded to a copper conductor layer by heat press. In this manufacturing process, as shown in Figure 2B, a PI film, a sheet adhesive (Parylux FR 1500; DuPont), and a copper foil were placed in sequence inside a heat press machine and heated for 1.5 h (195°C, 14–28 kg/cm^2). A layer of Teflon film was placed right above the PI film to avoid bonding with the rubber. Rubber sheets were placed on the bottom and top layers to make the heat and pressure homogeneous.

The insulation layer of the EPad was also manufactured by screen printing using a coating machine (MSK-AFA-ES200; SZKEJING). As shown in Figure 2C, the conductive substrate was first placed in the basement of the coating machine. Then LuxPrint paste was poured in front of the scraper on the conductive substrate. The scraper was controlled to move forward at 5 mm/s, and a thin layer of LuxPrint was left above the conductive substrate. By adjusting the gap height under the scraper, the thickness of the LuxPrint can be tuned. Next, LuxPrint was cured for 10 min at 130°C in an oven. Similarly, the carbon nanotube was coated on a polyurethane film by screen printing. The polyurethane film

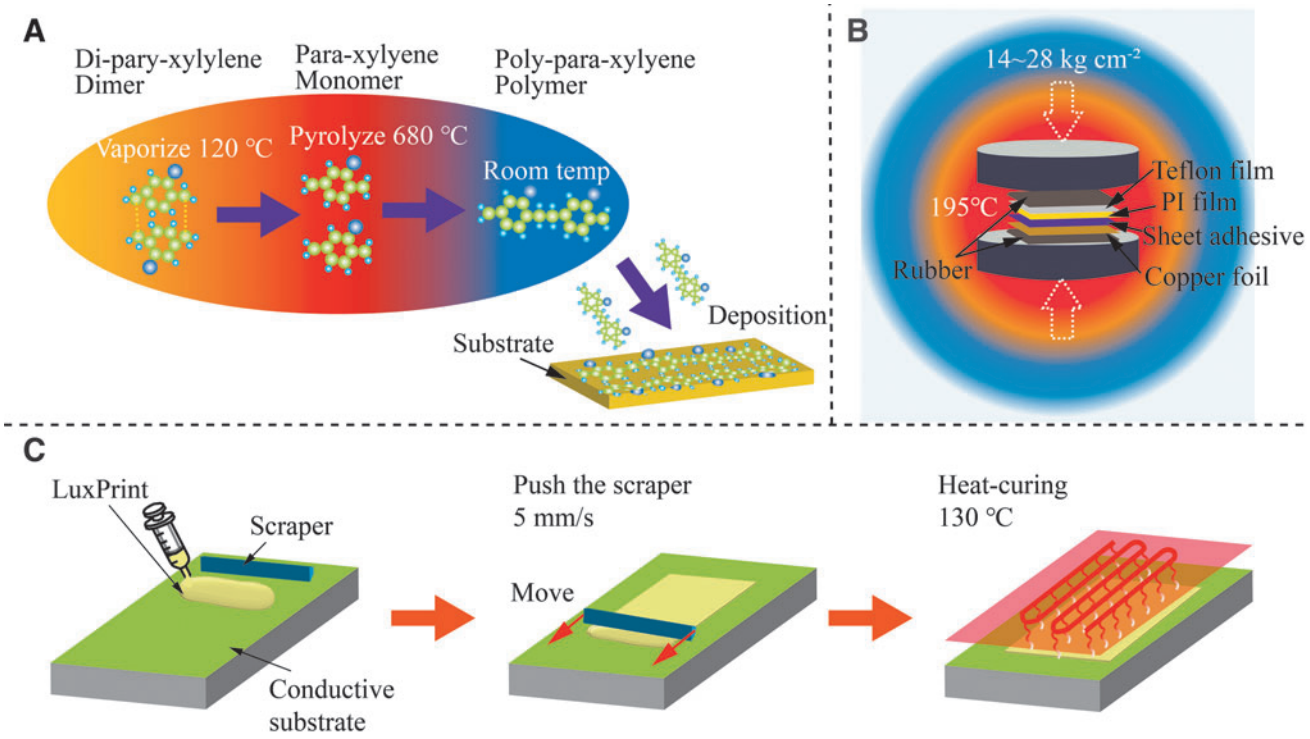

FIG. 2. The manufacturing methods in this study. **(A)** Parylene coating. **(B)** Heat and press PI films. **(C)** Screen printing of LuxPrint on the metal layer. PI, polyimide.

was first treated by air plasma (TS-PL02Z Plasma Cleaner; Tonson) for 2 min to generate a hydrophilic surface.

Then, the multiwalled carbon nanotube suspension (0.2% w/w; Timesnano) was poured in front of the scraper on the polyurethane film. Next, the scraper was moved forward, and a thin layer of the carbon nanotube suspension was left on the polyurethane film. After the solvent evaporated at room temperature (4 h), a thin layer of carbon nanotube was coated on the polyurethane film. In addition, the P(VDF-TrFE-CTFE) dielectric film (20 μm) was also coated on a copper film (7 μm) by a similar protocol. The P(VDF-TrFE-CTFE) film was prepared by dissolving the P(VDF-TrFE-CTFE) powder (Piezotech S.A., France) in *N,N*-dimethylformamide (DMF) with the ratio of 3 g: 20 mL.

Among the samples, BOPP film (25 μm) is coated with a layer of 70 nm aluminum using electroplating by the manufacturers.

Results

Modeling of electroadhesion

The conductive layer of the EPad and the conductive pad together consist of a parallel plate capacitor, as shown in Figure 1A. An electroadhesive force is generated between the two conductive plates, according to Coulomb's law. The tightly adherent pad produces resistance in the lateral direction, which can bear a heavy load. The electroadhesive force can be calculated by

$$F = \frac{1}{2}\varepsilon S\left(\frac{V}{d}\right)^2 = \frac{1}{2}\varepsilon S E^2, \tag{1}$$

where ε is the permittivity, S is the effective area, V is the voltage, d is the thickness of the insulator, and E is the electrical field. The adhesion force is proportional to the square of the voltage. If we can increase the driving voltage, the adhesive force can be drastically improved. In previous study, the practical voltage is usually much lower than the theoretical value due to the breakdown rising from the defects.[29] Increasing the driving voltage, the lateral force can be dramatically improved and withstand heavier loads. To achieve this goal, the self-clearing method is essential.

Modeling of self-clearing

A breakdown usually happens when the electrical field is higher than the dielectric strength of the insulation materials. In practice, the insulator is subject to electrical breakdown at the site of the defect over a voltage lower than the theoretical value since it causes a concentrated electrical field.[4,30] As shown in Figure 1C, various defects, including foreign particles, heterogeneous crosslinking, and uneven thickness of the insulation layer, always exist in EPads and limit the driving voltage. Based on the electronic avalanche theory, molecules at the defects are ionized during the dielectric breakdown of the insulator, as shown in Figure 1D.

A vast number of ions form an arc between conductors, accompanied by large Joule heat. This heat energy generated by the electricity evaporates the thin electrode nearby the breakdown site. Vaporization of the metal at the defect increases the resistance and reduces the arc duration. Eventually, the conductors are removed, the breakdown site is isolated from the circuit, and, finally, the circuit resumes regular operation. This process is called self-clearing since its recovery does not require external stimulation and operation.

In the process of clearing, the generated heat is mainly related to the current and voltage. The current through the arc is proportional to the voltage and inversely proportional to the ballast resistance. The arc is generally extinguished when the current is 0. In addition, the arc duration of self-clearing increases as the breakdown voltage increases, but it is difficult to build an analytical relationship with the voltage.[31,32] The discharge in the air is governed by hundreds of chemical reactions, and the energy required is highly dependent on the intrinsic properties of the materials, including the conductor and insulator.

The energy required for self-clearing is the combination of the energy of evaporation of the metal electrodes and the energy of decomposition and ionization of the dielectric polymer film, which is hard for quantitative analysis. Therefore, assuming that the current around the breakdown site is uniform, the surface current J and the power density P can be calculated by[33]:

$$J(\tau) = \frac{2I(\tau)}{\pi d_2}, \tag{2}$$

$$P(\tau) = \frac{I(\tau)^2\rho}{\pi d_2^2}, \tag{3}$$

where ρ is resistivity, d_2 is the channel diameter, τ is the arc duration, and $I(\tau)$ is the current during clearing. The current is decided by the resistance, and the resistance depends on the thickness of the conductors. Hence thicknesses of conductors are essential for generating different clearing modes.

In another aspect, the insulation layer thickness determines the breakdown voltage of electrostatic adhesion. During self-clearing, the clearing energy U_c is decided by the thickness of the conductor t and applied voltage V[29,34]:

$$U_c \propto V^4 t^2. \tag{4}$$

Therefore, the insulation layer thickness affects the clearing area consequently. According to the clearing power and current during the arcs, different thicknesses of conductors can generate different clearing modes.

During the breakdown, the temperature can rise to a high level in the limited zone. For example, a 7000 K temperature is observed in the previous study, and the boiling point of most metals and the decomposition temperature of insulation materials are far below this value.[35] Consequently, this temperature evaporates the conductors and decomposes the polymers easily.

Based on the ideal gas law:

$$PV = nRT, \tag{5}$$

where P is the pressure, V is the volume, T is the temperature, n is the number of moles, and R is the ideal gas constant. The generated gas produces a large pressure, and this pressure generates a bulge on the conductor layer. For example, the aluminum gas becomes 24,600 times larger than its solid

state, and the BOPP polymer becomes 42,110 times larger after vaporization and decomposition.[33]

Four clearing modes

In this study, we proposed four self-clearing modes to explain the different self-clearing phenomena in our experiments (Fig. 1E). In Mode I, the conductive layer is ultrathin, tens to hundreds of nanometers, and the conductor around the breakdown site is apt to be vaporized and generate an open channel easily. The metal around the defect is far away from the cleared channel, which not only avoids forming a conducting channel but also weakens the edge effect. In this case, lots of graphite, which is produced by decomposing the insulator,[33] is eliminated around the cleared area. The diameter of the breakdown channel is usually within 200 μm,[36] and the diameter of the nanometallization thin film is much larger than the diameter of the breakdown channel.

When the conductive layer becomes thicker (Mode II), the resistance actually decreases, and the increased current generates more heat during the arc. Consequently, an open channel is generated on the conductive layer in the breakdown site, similar to Mode I. Since the conductive layer is thicker, before generating an open channel in the conductor, the vaporized conductor and insulator transfer into the high-pressure gas in the conductive layer. Therefore, the pressured gas delaminates the conductor from the insulator surface and produces a bulge. The clearing succeeds in Mode I and Mode II.

When the conductive layer thickness continues to increase (Mode III), more insulator is vaporized, and more graphite is generated and left upon the wall of the breakdown hole. This graphite might not become a conductive layer (the graphite becomes conductive once its thickness is larger than 10 nm[29]), but it makes the breakdown hole less insulated and vulnerable to a second breakdown. This is a poor clearing.

Once the thickness increases to a large value (Mode IV), the heat energy is not adequate to vaporize the conductive layer on the breakdown site anymore, but the generated pressure from the cleared insulator can still generate a bulge on the conductive layer. In this clearing mode, although the polymer is removed around the breakdown site, most of the graphite is trapped inside the bulge. Thus, this is a failed clearing. These four proposed clearing modes are validated through the electrical performance and the morphology of EPads after self-clearing in the following descriptions.

Electrical performance of self-clearing

The electrical performance (voltage and current) can directly indicate the self-clearing process. For a failed self-clearing process, the short-circuit makes the current suddenly soar up to 11 mA from <0.1 mA, and the voltage simultaneously drops to several volts due to the power limitation of the amplifier, as shown in Figure 3A. With such a low voltage, according to Equation (1), the EPad cannot operate anymore.

With a successful clearing process, as shown in Figure 3B, after the breakdown, the current decreases drastically (in <150 μs) to <0.1 mA, and simultaneously the voltage recovers back to the regular magnitude. Consequently, the circuit survives, and the EPad can work again. This clearing and recovery process can repeat multiple times stably, as shown in Figure 3C. In another case, if the clearing quality is poor, a large amount of graphite is left on the clearing site and generates a conductive pathway due to the aggregation of graphite. Consecutive arcs happen at the same location.

Owing to the poor clearing and frequent breakdown, the voltage and current oscillate quickly, which is not acceptable for stable electrostatic adhesion (Fig. 3D). In addition, to demonstrate the broader application range of our self-clearing mechanism, we employed a thin flexible conductive layer carbon nanotube (thickness: 2 μm) onto a polyurethane film (thickness: 30 μm) to compose the EPad, and electrical behavior presents a successful self-clearing process, as shown in Supplementary Figure S1. In the experiments on EPads, the voltage was supplied by an amplifier (model 2220; Trek), which was controlled by a computer and a DAQ board (Cdaq-9174; NI).

The variation of voltage and current was recorded by an oscilloscope (Tektronix TBS1102) through the amplifier's monitor ports, and the statistical analysis and plotting were performed in Origin 2018. The surface topologies of EPads were observed by a confocal laser scanning microscope (VK-X1000; Keyence), and the image data were collected by using Keyence image-acquisition software (version 1.1.3.184).

Morphology of the EPads after self-clearing

With an ultrathin conductive layer (e.g., 70 nm aluminum), the cleared conductor is much larger than the cleared insulation layer, as shown in Figure 4A. Therefore, the circuit is isolated from the short site (Mode I). When the conductive layer is thicker (e.g.,7 μm copper), the conductive layer of the EPad bumps up to around the breakdown site due to the uneven strain resulting from the ambient temperature and gas pressure coming from the vaporized insulator. The deformed conductor sections become far away from the short site, extinguishing the arc, as shown in Figure 4B and Supplementary Figure S2 (Mode II).

In another case, the conductive layer with a copper layer of 7 μm or thicker has black graphite remaining on the insulation layer around the breakdown site (Fig. 4C). This is a poor clearing—the remained graphite results in consecutive arcs (Mode III). When the conductive layer is too thick (e.g., 15 μm copper), the conductive layer has no hole generated by the arc at all, as shown in Figure 4D. The energy during the breakdown is not adequate to evaporate the thick metal, and graphite decomposed from the insulator is trapped on the insulation (Mode IV).

It seems that a thinner conductive layer is more likely to induce successful self-clearing. Still, the ultrathin conductive layer also forms a sharp edge and causes an electrical field concentration and breakdown through the air. We verify the electrical field concentration phenomenon by the simulated result (COMSOL 5.6) of the sandwiched structure, a 70 nm aluminum layer, a 20 μm insulated layer (dielectric constant: 2.2), and a 10 μm copper layer when applying 100 V to the top layer, as shown in Supplementary Figure S3.

In the EPad with a 70 nm aluminum layer, consecutive breakdowns along the edges happen before it occurs at the center. Consequently, the EPad practical maximum voltage and adhesive force are much lower than the theoretical values. A tradeoff between the clearing effect and edge effect should be considered when we select the thickness of the conductive layer. The self-clearing of the two conductors of the electrostatic adhesion can ensure a better recovery of the device.

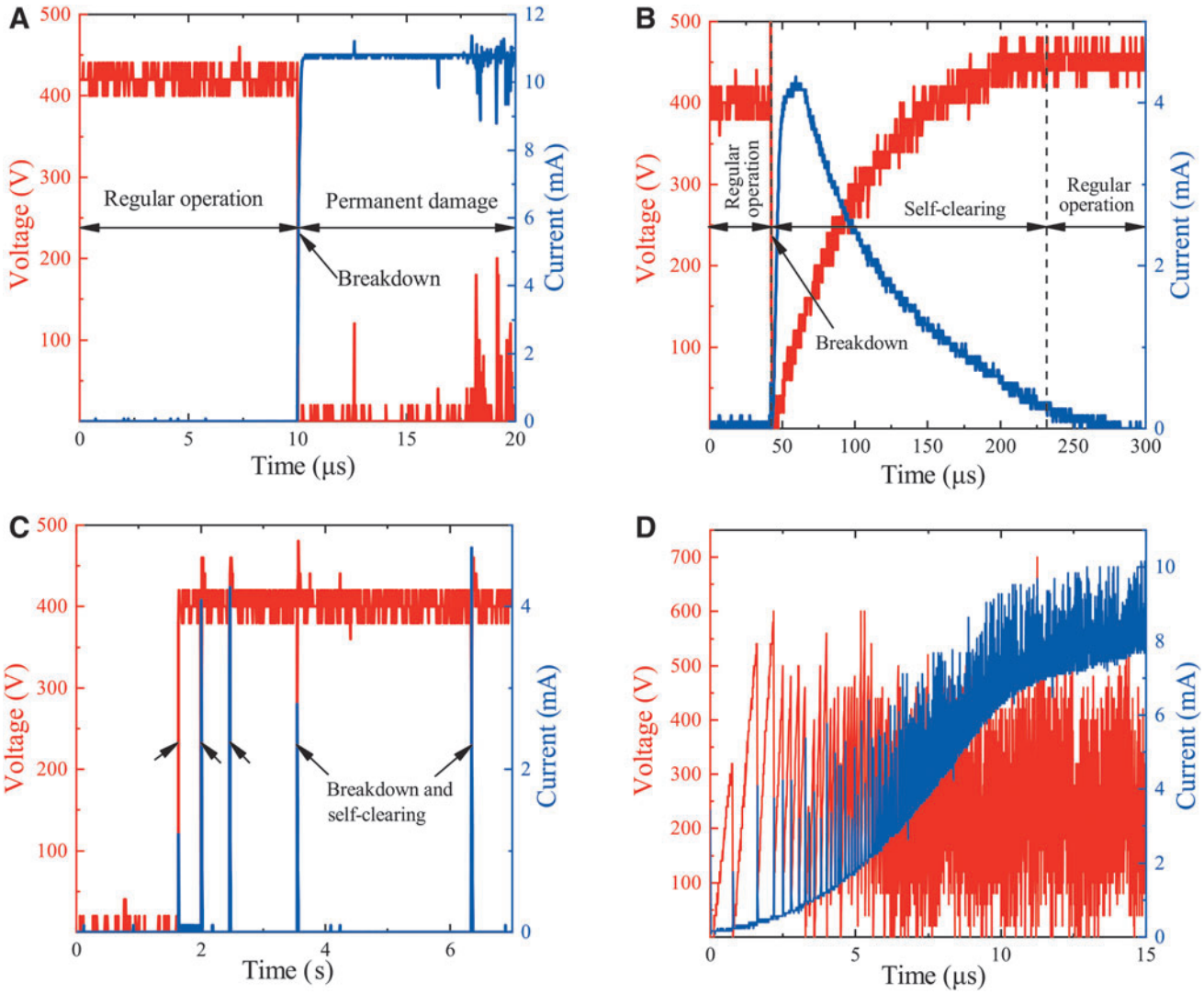

FIG. 3. The electrical performance (voltage and current) for an EPad with or without self-clearing. **(A)** Short circuit without self-clearing (parylene thickness: 5 μm, copper thickness: 15 μm). **(B)** Once successful self-clearing process (parylene thickness: 5 μm, copper thickness: 7 μm). **(C)** Multiple successful self-clearing processes (parylene thickness: 5 μm, copper thickness: 7 μm). **(D)** Poor self-clearing process (parylene thickness: 2.5 μm, copper thickness: 7 μm). EPad, electroadhesive pad.

Influence of the insulation layer thickness

In another aspect, the insulation layer thickness of EPads determines various other features of the self-clearing such as the theoretical breakdown voltage, clearing area, and the number of breakdown sites. When the EPads are supplied with a stepped increasing voltage shown in Figure 5A, in this study, the first breakdown voltage is almost the same for the insulator layer of 5 and 7 μm thickness due to the defects, while theoretically, the latter should be 1.4 times larger. In previous research, this magnitude is usually set as the threshold to avoid failure.

However, owing to the self-clearing mechanism, the EPad in this study survives after the first breakdown and earns a higher critical voltage since the weakest point (defect) is removed. The maximum voltage increases by 160% (7 μm insulation layer) at least and 260% (2.5 μm insulation layer) at maximum, as shown in Figure 5B. This means the adhesive force could increase by 676% at maximum, according to Equation (1).

As shown in Figure 5C, the insulator of 2.5 μm thickness has 94 times more breakdown sites than that of 7 μm thickness, perhaps because thicker holes have larger exposed areas and retain more graphite, which causes the following breakdown at the same site. Moreover, as shown in Figure 5D, the clearing area on both the conductive layer and the insulation layer gently grows when the insulation layer becomes thicker, perhaps because thicker insulation induces a higher breakdown voltage and more energy in the breakdown. The difference between the cleared area of the conductor and the insulator can be represented by the clearing ratio m:

$$m = \frac{d_1 - d_2}{d_2}, \tag{6}$$

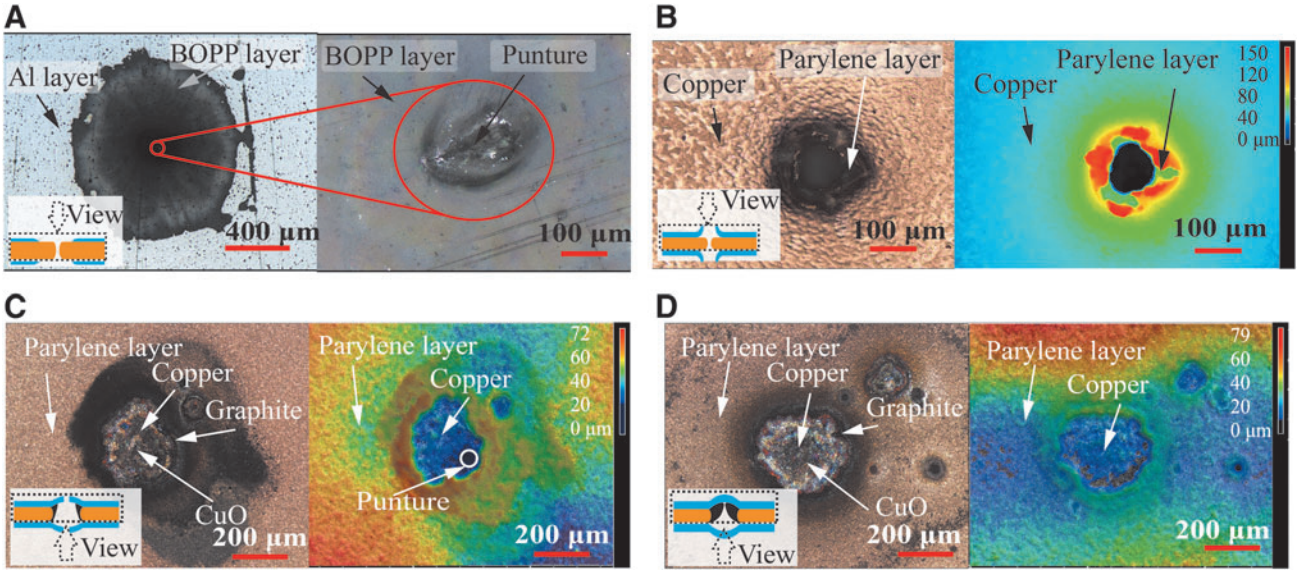

FIG. 4. The surface morphology of the EPads after electric breakdowns. **(A)** Self-clearing of an EPad (25 μm BOPP and 70 nm aluminum). **(B)** Self-clearing of an EPad (7 μm parylene C and 7 μm copper). **(C)** Poor self-clearing of an EPad (7 μm parylene C and 7 μm copper). **(D)** Failed self-clearing of an EPad (7 μm parylene C and 15 μm copper). BOPP, biaxially oriented polypropylene.

where d_1 and d_2 are the diameters of the cleared area on the conductive layer and insulation layer, respectively. In the test of different insulation layer thicknesses, we set the thickness of the conductive layer constant, 7 μm (copper), but differ in the insulation layer thickness (2.5, 5, and 7 μm, respectively, parylene). As shown in Figure 5E, with the increase of the insulator thickness, the clearing ratio rises, which means it becomes safer since the remaining conductor becomes further from the breakdown site.

Therefore, the thinner insulation layer causes significantly more breakdown sites and a slightly smaller clearing area. Consequently, the effective adhesive area is reduced. As shown in Figure 5F, when the insulator thickness is merely 2.5 μm, the lateral force after clearing drops by $\sim$20%. In contrast, the force decrease is <1% for the insulation with a thickness of 5 or 7 μm.

Influence of the insulation materials

The material of the insulation layer also fundamentally affects the self-clearing by limiting the dielectric strength and, therefore, the theoretical breakdown voltage and maximum adhesive force [according to Eq. (1)], as shown in Figure 1B. Moreover, the materials restrict the manufacturing methods and the available thickness of the insulation layer to influence the self-clearing in multiple aspects, as aforementioned. Besides, different insulation materials generate various surface morphologies.

For example, the roughness (*R*a) of Luxpint insulation is larger than 0.06 μm due to the large particles of $BaTiO_3$, whereas that of other materials, such as PI, parylene, and BOPP in this study, is <0.01 μm. The high roughness increases the coefficient of friction and brings more unevenness to the surface causing a concentrated electrical field between the conductive pad and EPad.

Self-clearing can benefit electrostatic adhesion in various aspects, including its performance and reliability, which are both critical for practical applications. As shown in Figure 1B, with the same material, we can achieve 276% times higher force for PI, 237% for parylene, and 133% for $BaTiO_3$ than the maximum value from previous study, respectively. The lateral electroadhesive force was measured using a tensile tester (990B; ZHIQU) to pull the EPad to move relative to the conductive pad.

The repeatability of self-clearing

To demonstrate the repeatability and reliability of self-clearing, we prepared an EPad composed of a copper layer (7 μm) and a P(VDF-TrFE-CTFE) layer (20 μm) for the multiple breakdown test. A stepped increasing voltage was supplied to the EPad with a 10 V increment, and each step lasted 15 min. The applied voltage was first increased to 470 V, under which the breakdown was initiated. Each peak of the current response represents a successful self-clearing, as shown in Figure 5G. After surviving 173 times and 65-min consecutive sparks, several long-last short circuits occurred on the voltage of 510 V, which accompanied large-area breakdown sites (Supplementary Fig. S4) and resulted in the failure of the EPad.

The long-last short circuit may be caused by the uneven distribution of the dielectric layer or the open channel (single breakdown site) for the air breakdown. The robustness and long continuous working capacity of the EPad demonstrate the good repeatability of self-clearing.

Applications of EPads with self-clearing

As shown in Figure 6A–C and Supplementary Videos S1–S3, suffering penetration, punching, and cutting, the EPad survived with the self-clearing mechanism. The clearing process completes so quickly, and it takes little effect on the regular operation of electrostatic adhesion. As shown in Figure 6D and Supplementary Video S4, the electrostatic clutch held a weight of 200 g under it. Although sparks and

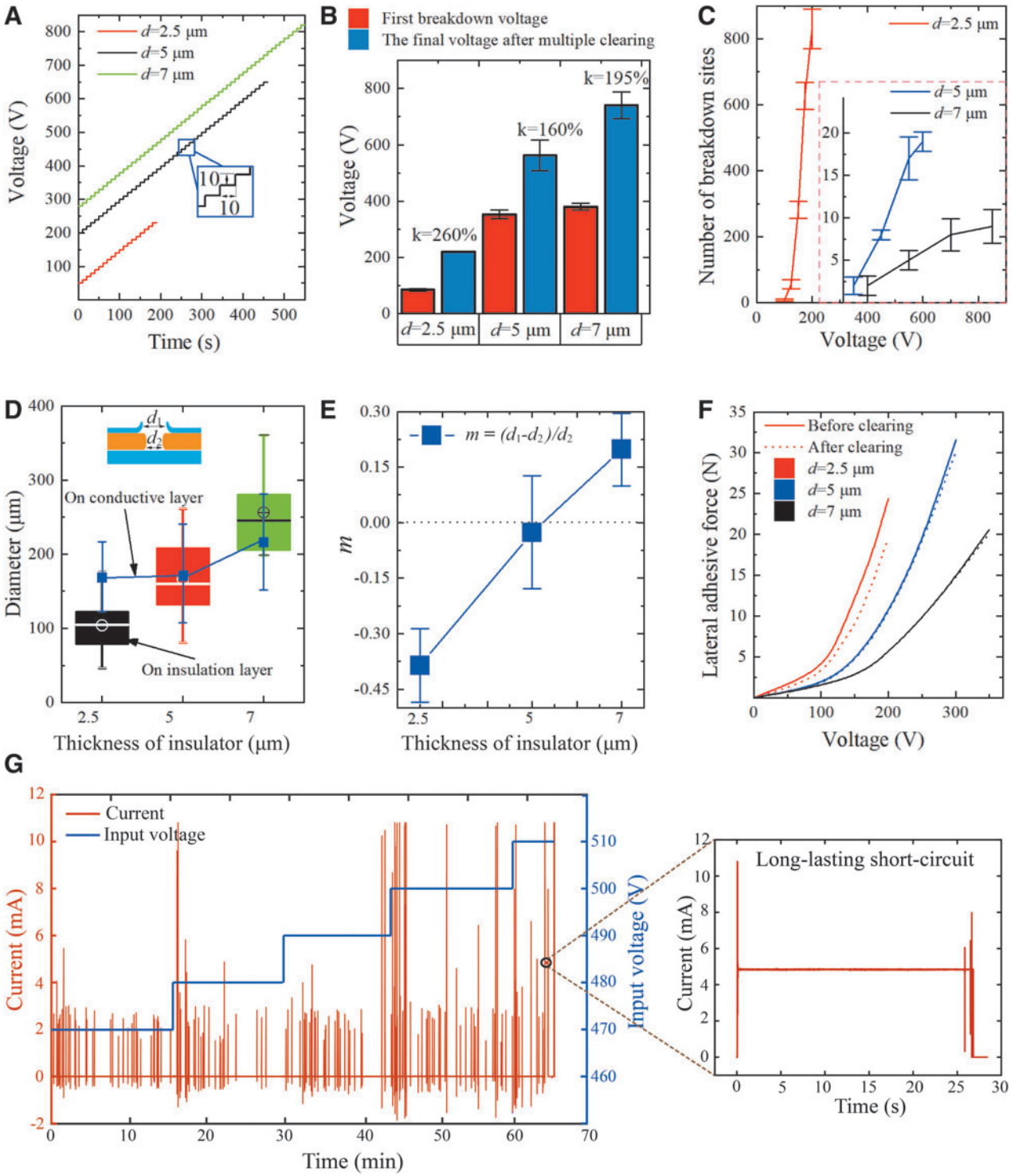

FIG. 5. The influence of the EPad insulation layer thickness. **(A)** The supplied voltage during the electric breakdown test. **(B)** Maximum voltages before and after multiple self-clearing. k is the ratio between the maximum voltage before and after the clearing for the same thickness. **(C)** The number of breakdown sites at different insulator thicknesses. **(D)** The diameters of the cleared area on the conductive layer and insulation layer of EPads for different parylene coating thicknesses. **(E)** The clearing ratio m for different parylene coating thicknesses. d_1 is the diameter of the breakdown site in the conductive layer and d_2 is the diameter of the breakdown site in the insulation layer. **(F)** The lateral electrostatic adhesive force before and after self-clearing. **(G)** The current behavior of the repeatability test for self-clearing and the inset presents a long-last short-circuit process.

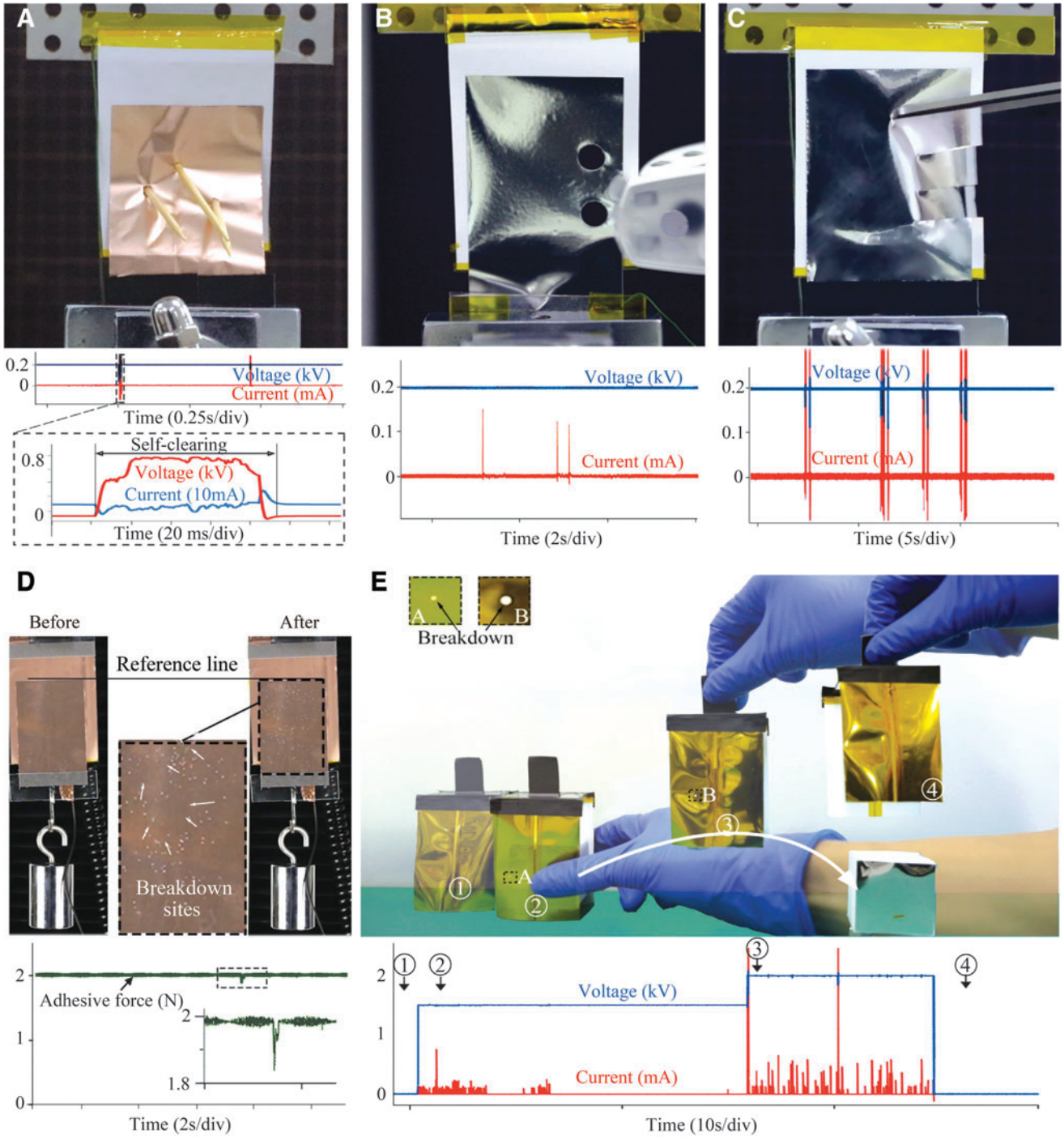

FIG. 6. The reliability of electrostatic adhesive devices resulted from the self-clearing mechanism. The electrostatic clutch survives severe physical damages, such as **(A)** penetration using tooth sticks, **(B)** punching, and **(C)** cutting. The current and voltage are shown, respectively, and their spikes represent the short circuit and self-clearing. **(D)** The stability of the electrostatic clutch while holding a weight of 200 g. The force on the EPad is measured by a load cell (not shown in this figure) connected above the EPad. The lateral force is shown below. **(E)** An electrostatic gripper is completing a pick-and-place task, although electrical breakdown happens. The voltage and current are shown below.

short circuits were generated intentionally by increasing the voltage, the clutch kept at the same position and recovered quickly after the self-clearing process.

Finally, we demonstrated the applications of self-cleaning with a more practical scenario of pick and place. The gripper is made of two EPads. In previous study, when a spark was generated, the gripper lost all the force due to a short circuit. This failure comes suddenly and unpredictably and might result in an accident of dropping the object. On the contrary, with self-clearing, as shown in Figure 6E and Supplementary Video S5, the gripper first survived the electrical breakdown at State 2 (1500 V) and recovered back instantaneously from

the increased applied voltage at State 3 (2000 V), resulting in slight fluctuation in the gripping and transferring process, which presents the reliability of our self-clearing mechanism.

Conclusions

In this study, we propose a self-clearing method—simply employing an enough thin conductive layer to allow the arc energy to evaporate the defects on the EPads—to promote the force and reliability of electrostatic adhesion. This study builds the qualitative models for the self-clearing phenomenon and proposes four clearing modes to understand the clearing results, mainly depending on the different thicknesses of the conductive layer, which are verified by the microscopic surface morphology and the electrical performance during and after the clearing. Our tests demonstrate that this clearing mechanism requires no other new materials and fabrication process, and it is valid, economical, and easy to operate.

According to the high-energy arcs during the self-clearing process, defects are eliminated, and the cleaned holes are generated to prevent further breakdowns. After clearing, the working voltage is increased to 260%, which means that the lateral force can be significantly increased (by 276% in our tests), and accidental short currents on EPads can be avoided. In addition, the cleaned area is relatively small, so it has little effect on the lateral force.

Moreover, the repeatability and reliability of self-clearing are verified by surviving 173 times and 65-min consecutive sparks during the electric breakdown test. Finally, we demonstrated an EPad survived severe physical damages (such as punctures, penetrations, and cuttings), and an EPad clutch exhibited stable and reliable operations by holding a 200 g weight and presented a stable pick-and-place operation by an EPad gripper with self-clearing.

Our self-clearing mechanism enables more practical and extensive applications on EPads, such as gripping and clutching, and benefits other electrostatic-based actuations, such as dielectric elastomer actuators and piezoelectric polymer actuators. Versatile conductive materials, including conductive polymers and carbon nanotubes, may also be involved to enrich self-clearing. In the future, we will explore more potential applications based on this mechanism.

Author Disclosure Statement

No competing financial interests exist.

Funding Information

This study was supported in part by the National Key R&D Program of China under Grant No. 2022YFB4701200, in part by the National Natural Science Foundation of China under Grant No. 52275021, in part by the Science, Technology, and Innovation Commission of Shenzhen Municipality under Grant No. ZDSYS20200811143601004, in part by the Natural Science Foundation of Liaoning Province of China (State Key Laboratory of Robotics joint funding, under Grant No. 2021-KF-22-11), and in part by Southern Marine Science and Engineering Guangdong Laboratory (Guangzhou) under Grant No. K19313901.

Supplementary Material

Supplementary Figure S1
Supplementary Figure S2
Supplementary Figure S3
Supplementary Figure S4
Supplementary Video S1
Supplementary Video S2
Supplementary Video S3
Supplementary Video S4
Supplementary Video S5

References

1. Guo J, Leng J, Rossiter J. Electroadhesion technologies for robotics: a comprehensive review. IEEE Trans Robot 2019; 36:313–327.
2. Liu R, Chen R, Shen H, *et al.* Wall climbing robot using electrostatic adhesion force generated by flexible interdigital electrodes. Int J Adv Robot Syst 2013;10:36.
3. Ruffatto III D, Parness A, Spenko M. Improving controllable adhesion on both rough and smooth surfaces with a hybrid electrostatic/gecko-like adhesive. J R Soc Interface 2014;11:20131089.
4. Gu G, Zou J, Zhao R, *et al.* Soft wall-climbing robots. Sci Robot 2018;3:eaat2874.
5. Qin L, Liang X, Huang H, *et al.* A versatile soft crawling robot with rapid locomotion. Soft robotics 2019;6:455–467.
6. Graule M, Chirarattananon P, Fuller S, *et al.* Perching and takeoff of a robotic insect on overhangs using switchable electrostatic adhesion. Science 2016;352:978–982.
7. Park S, Drew DS, Follmer S, *et al.* Lightweight high voltage generator for untethered electroadhesive perching of micro air vehicles. IEEE Robot Autom Lett 2020;5:4485–4492.
8. Hinchet R, Vechev V, Shea H, *et al.* Dextres: Wearable haptic feedback for grasping in vr via a thin form-factor electrostatic brake. In: Proceedings of the 31st Annual ACM Symposium on User Interface Software and Technology. Berlin, Germany: Association for Computing Machinery (ACM), 2018, pp. 901–912.
9. Xiong Q, Liang X, Wei D, *et al.* So-EAGlove: VR haptic glove rendering softness sensation with force-tunable electrostatic adhesive brakes. IEEE Trans Robot 2022;38: 3450–3462.
10. Diller S, Majidi C, Collins SH. A lightweight, low-power electroadhesive clutch and spring for exoskeleton actuation. In: 2016 IEEE International Conference on Robotics and Automation (ICRA). Stockholm, Sweden: IEEE, 2016, pp. 682–689.
11. Ramachandran V, Shintake J, Floreano D. All-fabric wearable electroadhesive clutch. Adv Mater Technol 2019; 4:1800313.
12. Detailleur A, Umans S, Van Even H, *et al.* Feasibility analysis of a self-reinforcing electroadhesive rotational clutch. In: 2021 IEEE/ASME International Conference on Advanced Intelligent Mechatronics (AIM). Delft, Netherlands: IEEE, 2021; pp. 478–483.
13. Schaler EW, Ruffatto D, Glick P, *et al.* An electrostatic gripper for flexible objects. In: 2017 IEEE/RSJ International Conference on Intelligent Robots and Systems (IROS). Vancouver, BC, Canada: IEEE, 2017, pp. 1172–1179.
14. Shintake J, Rosset S, Schubert B, *et al.* Versatile soft grippers with intrinsic electroadhesion based on multifunctional polymer actuators. Adv Mater 2016;28:231–238.

15. Cao C, Sun X, Fang Y, *et al.* Theoretical model and design of electroadhesive pad with interdigitated electrodes. Mater Des 2016;89:485–491.
16. Coulson R, Stabile CJ, Turner KT, *et al.* Versatile soft robot gripper enabled by stiffness and adhesion tuning via thermoplastic composite. Soft Robotics 2021. [Epub ahead of print]; DOI: 10.1089/soro.2020.0088
17. Hwang G, Park J, Cortes DSD, *et al.* Electroadhesion-based high-payload soft gripper with mechanically strengthened structure. IEEE Trans Ind Electron 2021;69:642–651.
18. Gao X, Cao C, Guo J, *et al.* Elastic electroadhesion with rapid release by integrated resonant vibration. Adv Mater Technol 2019;4:1800378.
19. Yu J, Chary S, Das S, *et al.* Gecko-inspired dry adhesive for robotic applications. Adv Funct Mater 2011;21:3010–3018.
20. Yoshida Y, Ma S, editors. Design of a wall-climbing robot with passive suction cups. In: 2010 IEEE International Conference on Robotics and Biomimetics. Tianjin, China: IEEE, 2010, pp. 1513–1518.
21. Berengueres J, Tadakuma K, Kamoi T, *et al.* Compliant distributed magnetic adhesion device for wall climbing. In: Proceedings 2007 IEEE International Conference on Robotics and Automation (ICRA). Rome, Italy: IEEE, 2007, pp. 1256–1261.
22. Xie G, Wang W, Zhao X, *et al.* Low-voltage electroadhesive pad with thin insulation layer fabricated by parylene deposition. In: 2019 IEEE 9th Annual International Conference on CYBER Technology in Automation, Control, and Intelligent Systems (CYBER). Suzhou, China: IEEE, 2019; pp. 197–202.
23. Diller SB, Collins SH, *et al.* The effects of electroadhesive clutch design parameters on performance characteristics. J Intell Mater Syst Struct 2018;29:3804–3828.
24. Zakrevskii V, Pakhotin V, Sudar N. Ageing and breakdown of thin insulating polymer films. J Appl Phys 2014;115:234101.
25. Young AL, Hilmas GE, Zhang SC, *et al.* Mechanical vs. electrical failure mechanisms in high voltage, high energy density multilayer ceramic capacitors. J Mater Sci 2007;42:5613–5619.
26. Stoyanov H, Brochu P, Niu X, *et al.* Lifetime, fault-tolerant freestanding actuators based on a silicone dielectric elastomer and self-clearing carbon nanotube compliant electrodes. RSC Adv 2013;3:2272–2278.
27. Yuan W, Hu L, Yu Z, *et al.* Fault-tolerant dielectric elastomer actuators using single-walled carbon nanotube electrodes. Adv Mater 2008;20:621–625.
28. Zhang Y, Ellingford C, Zhang R, *et al.* Electrical and mechanical self-healing in high-performance dielectric elastomer actuator materials. Adv Funct Mater 2019;29:1808431.
29. Ahmed S, Ounaies Z, Lanagan MT. On the impact of self-clearing on electroactive polymer (EAP) actuators. Smart Mater Struct 2017;26:105024.
30. Wang H, Yamamoto A. A thin electroadhesive inchworm climbing robot driven by an electrostatic film actuator for inspection in a narrow gap. 2013 IEEE International Symposium on Safety, Security, and Rescue Robotics(SSRR). Linköping, Sweden: IEEE, 2013, pp. 1–6.
31. Tortai J, Denat A, Bonifaci N. Self-healing of capacitors with metallized film technology: experimental observations and theoretical model. J Electrostat 2001,53:159–169.
32. Bel'Ko V, Bondarenko P, Emel'Yanov O. The dynamic characteristics of self-healing processes in metal film capacitors. Russ Electr Eng 2007,78:138–142.
33. Qin S, Ma S, Boggs SA. The mechanism of clearing in metalized film capacitors. In: 2012 IEEE International Symposium on Electrical Insulation. San Juan, PR, USA: IEEE, 2012, pp. 592–595.
34. Shaw D, Cichanowski S, Yializis A. A changing capacitor technology-failure mechanisms and design innovations. IEEE Trans Electr Insul 1981;16:399–413.
35. Tortai J, Bonifaci N, Denat A, *et al.* Self-healing of aluminium metallized polypropylene films: a spectroscopic investigation. In: Proceedings of 2002 IEEE 14th International Conference on Dielectric Liquids ICDL. 2002, Graz, Austria: IEEE, pp. 190–193.
36. Budenstein PP. On the mechanism of dielectric breakdown of solids. IEEE Trans Electr Insul 1980;15:225–240.

Address correspondence to:
Hongqiang Wang
Shenzhen Key Laboratory
of Biomimetic Robotics and Intelligent Systems
Department of Mechanical and Energy Engineering
Southern University of Science and Technology
No. 1088, Xueyuan Boulevard
Nanshan District
Shenzhen 518055
China

E-mail: wanghq6@sustech.edu.cn